Regular Article

Effect of Si content on the thermoelectric transport properties of Ge-doped higher manganese silicides

CrossMark

Hwijong Lee [a], Gwansik Kim [a], Byunghun Lee [a], Jeongmin Kim [a], Soon-Mok Choi [b], Kyu Hyoung Lee [c,**], Wooyoung Lee [a,*]

[a] Department of Materials Science and Engineering, Yonsei University, Seoul 03722, South Korea
[b] School of Energy, Materials and Chemical Engineering, Korea University of Technology and Education, Cheonan 31253, South Korea
[c] Department of Nano Applied Engineering, Kangwon National University, Chuncheon 24341, South Korea

ARTICLE INFO

ABSTRACT

Polycrystalline bulks of Si-content tuned Ge-doped higher manganese silicides (HMSs) were fabricated to elucidate the effects of Si content on the phase formation behavior and thermoelectric properties. The phase formation and electronic transport characteristics of HMSs were significantly dependent on Si content. Improved power factor was obtained at higher Si contents because of an enhanced Seebeck coefficient due to the increase in density of states effective mass, maintaining electrical conductivity. Furthermore, the lattice thermal conductivity was reduced through Si-content tuning, which suppressed the formation of secondary phases. Thus, a maximum ZT of 0.61 at 823 K was obtained in $MnSi_{1.77}Ge_{0.027}$.

© 2017 Acta Materialia Inc. Published by Elsevier Ltd. All rights reserved.

1. Introduction

Thermoelectric power generation (TEG) is one of the most promising technologies for renewable energy generation owing to the direct conversion of heat to electrical energy. Recently, applications involving a TEG system have been focused on recovering waste heat from automobiles and industries because of the increasing societal need for high-efficiency energy use. The energy conversion efficiency of a TEG system is directly determined by the temperature difference and the dimensionless figure of merit ZT ($= \sigma S^2 T/\kappa$, where σ is the electrical conductivity, S is the Seebeck coefficient, κ is the total thermal conductivity, and T is the absolute temperature) of TE materials. Several TE materials including skutterudite-, [1,2] half-Heusler-, [3] and Si-based alloys [4,5] have been considered as promising candidates for mid-to-high temperature power generation applications owing to their high ZT and good chemical stability. Si-based alloys are more favorable for a TEG system owing to their earth-abundant and non-toxic constituents (Mg, Mn, and Si); however, it is necessary to obtain excellent TE performance, which implies a high ZT, particularly in p-type materials to ensure economic feasibility.

Transition metal silicides such as Fe-Si, Cr-Si, and Mn-Si have been intensively investigated as p-type Si-based TE materials owing to their low and anisotropic thermal conduction behavior and good chemical stability even at higher temperatures [6–8]. Among these materials, higher manganese silicides (HMSs) with a crystal structure known as the Nowotny chimney ladder (NCL) have high flexibility in terms of composition (Mn to Si ratio) owing to the different periodicity of the Si atoms and their modulation [9]. HMSs consist of a Mn sublattice and an interpenetrating helical Si sublattice and form four distinct phases, namely, Mn_4Si_7, $Mn_{11}Si_{19}$, $Mn_{15}Si_{26}$, and $Mn_{27}Si_{47}$. In HMSs, the substitutional doping approach has proven to be one of the effective ways to improve ZT as this approach can either improve the power factor (σS^2), due to the modification of electronic structure, or reduce the lattice thermal conductivity (κ_{lat}), due to intensified point-defect phonon scattering [10–17]. For example, Ge has been reported as the most effective doping element to induce point defects on Si substrates for simultaneous enhancement of carrier transport and phonon scattering [10–12]. On the other hand, controlling the phase formation behavior of HMSs is another key issue for obtaining high ZT, since the presence of secondary phases (MnSi and Si) and self-defects (Si vacancy) have effects on the electronic and thermal transport properties of HMSs. A previous study [13] reported that the formation of nano-scale (100–200 nm) metallic MnSi platelets gives arise to enhanced electronic transport properties of HMSs, originating from an increased electrical conductivity due to the increase in carrier concentration without a reduction in the carrier mobility. However, little is known about the

effects of Si content on the phase formation behavior, related with TE properties.

In the present study, we fabricated Ge-doped HMS polycrystalline bulks with controlled Si content expecting that it could manipulate the carrier and phonon transport properties of HMSs. An enhanced thermoelectric power generation (TEG) (~1.77 mW m^{-1} K^{-2} at 823 K) and a reduced κ_{lat} (~1.75 W m^{-1} K^{-1} at 823 K) resulting from the compositional tuning effect were simultaneously obtained by the optimization of Si content, and a maximum ZT of 0.61 at 823 K was achieved in MnSi$_{1.77}$Ge$_{0.027}$.

2. Experiment

Ge-doped HMS polycrystalline bulks (Ge-HMSs) with compositions MnSi$_{1.70 + x}$Ge$_{0.027}$ (x = 0, 0.03, 0.05, 0.07, and 0.1) were synthesized by combining a conventional solid-state reaction (SSR) and spark plasma sintering (SPS) using high purity elemental Mn (99.95%, Alfa Aesar), Si (99.9%, Alfa Aesar), and Ge (99.999%, Sigma Aldrich). The amount of Ge was kept constant at a value of 0.027, which was calculated based on 1 at% of the entire composition [10–12]. Pristine (undoped) MnSi$_{1.727}$ (or Mn$_{11}$Si$_{19}$) was synthesized by the same process. The stoichiometric materials mixed in an agate mortar were placed in a tube-type furnace; they were heat-treated at 1273 K for 24 h under dynamic vacuum and cooled to room temperature. The samples thus obtained were ground into a powder by conventional ball milling and sieved under 53 μm in mesh size. Then, bulk samples with a 10 mm diameter and thickness were prepared by SPS under 60 MPa, at 1193 K for 5 min under vacuum.

Phase analysis of the bulk samples prepared by SPS was carried out using powder X-ray diffraction (PXRD, Ultima IV/ME 200DX, Rigaku, Japan) with CuKα radiation. Structural factors obtained from the XRD data were calculated using Rietveld refinement. To measure σ, S, and κ in the same direction, square-shaped samples (6 mm × 6 mm × 1.2 mm) for thermal diffusivity measurements and bar-shaped samples (2 mm × 2 mm × 8 mm) for σ and S measurements were cut on a plane parallel and perpendicular to the SPS press direction, respectively. The σ and S values from 300 K to 873 K were measured using a TE property measurement system (ZEM-3, ULVAC, Japan) in a He atmosphere. Hall effect measurements were performed in the van der Pauw configuration under a constant magnetic field (1 T). Owing to the high Hall carrier concentration (p_H) of the Ge-HMSs, the Hall mobility (μ_H) was calculated using a single parabolic band (SPB) model without considering the minority carriers. The κ values were calculated using the equation $\kappa = DC_p\rho$, where ρ is the bulk density of the sample, D is the thermal diffusivity measured by using a laser flash method (Netzsch LFA-457, Germany), and C_p is the specific heat measured by using differential scanning calorimetry (DSC 8000, Perkin Elmer, USA).

3. Results and discussion

According to the stacking period difference, four distinct HMSs (Mn$_4$Si$_7$, Mn$_{11}$Si$_{19}$, Mn$_{15}$Si$_{26}$, and Mn$_{27}$Si$_{47}$) are formed, indicating that the ratio of Mn/Si is a critical factor influencing the crystal structure. Fig. 1 shows the XRD patterns for the bulks of pristine MnSi$_{1.727}$ and Ge-doped MnSi$_{1.70 + x}$ (Ge-HMSs) obtained by SPS. All major peaks are indexed to MnSi$_{1.727}$, while MnSi and Si are detected as secondary phases in all compounds. To clarify the phase formation behavior with varying Si content, we calculated the actual wt% of secondary phases using Rietveld refinement, as given in Table 1. Interestingly, the amounts of MnSi are significantly decreased with increasing Si content, suggesting that the additional Si is effective in suppressing the generation of MnSi by the acceleration of following reaction: MnSi + xSi → MnSi$_{1.727}$. However, at a higher Si content (MnSi$_{1.80}$Ge$_{0.027}$), the wt% of Si (~1.22 wt%) increases owing to the limit of occupancy on the Si site. These results suggest that the phase formation behavior of the HMSs could be controlled by adjusting the Si content of the starting
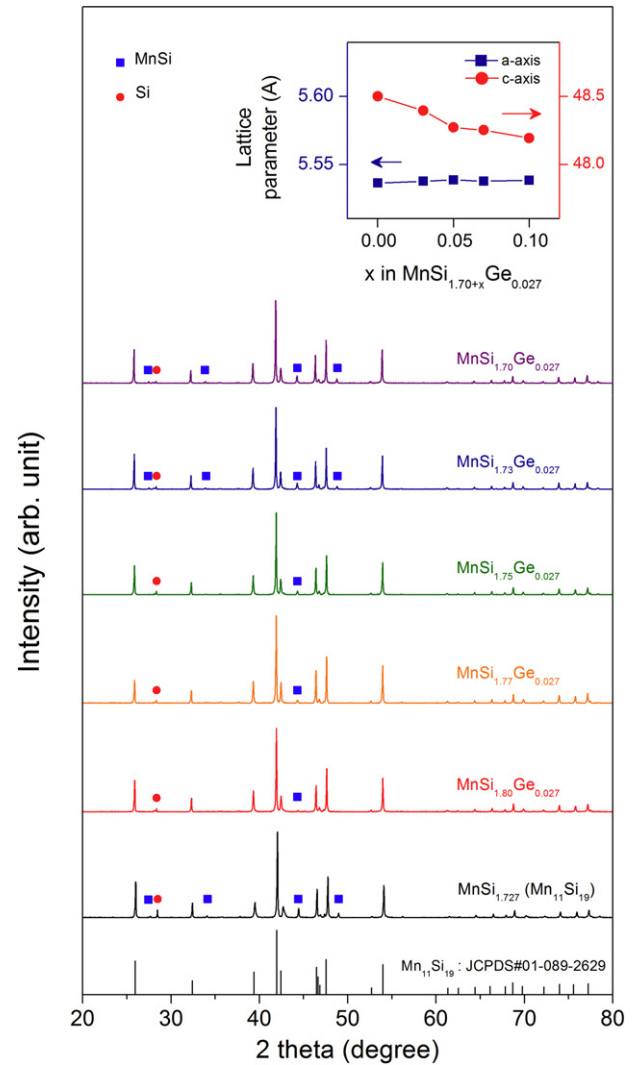

Fig. 1. Powder XRD patterns of SPSed HMS samples (Ge-HMSs and pristine MnSi$_{1.727}$) and the variation of lattice parameters (a and c) with Si content (inset).

materials. To further explain this phenomenon, we calculated the variation of lattice parameters (a and c) with Si content (inset of Fig. 1). It is noted that the values of lattice parameter a are almost the same for all Ge-HMSs, while the values of c monotonously decrease with increasing Si content. The formation of Si-content tuned HMSs with different Si-site occupancies is further confirmed from the fact that the lattice parameter for the [Si]-sublattice along the c–axis tends to decrease from 2.537 Å (Mn$_{11}$Si$_{19}$) to 2.495 Å (Mn$_4$Si$_7$) when the Mn to Si ratio increases [9].

To clarify the effects of Ge-doping and Si content on the electronic transport properties of HMSs, we measured the temperature dependences of σ and S (Fig. 2(a)) and p_H and μ_H values at 300 K (Table 2). All Ge-HMSs exhibit a σ value higher than that of pristine MnSi$_{1.727}$

Table 1
Amounts of calculated secondary phases (MnSi, Si) and densities for MnSi$_{1.70 + x}$Ge$_{0.027}$.

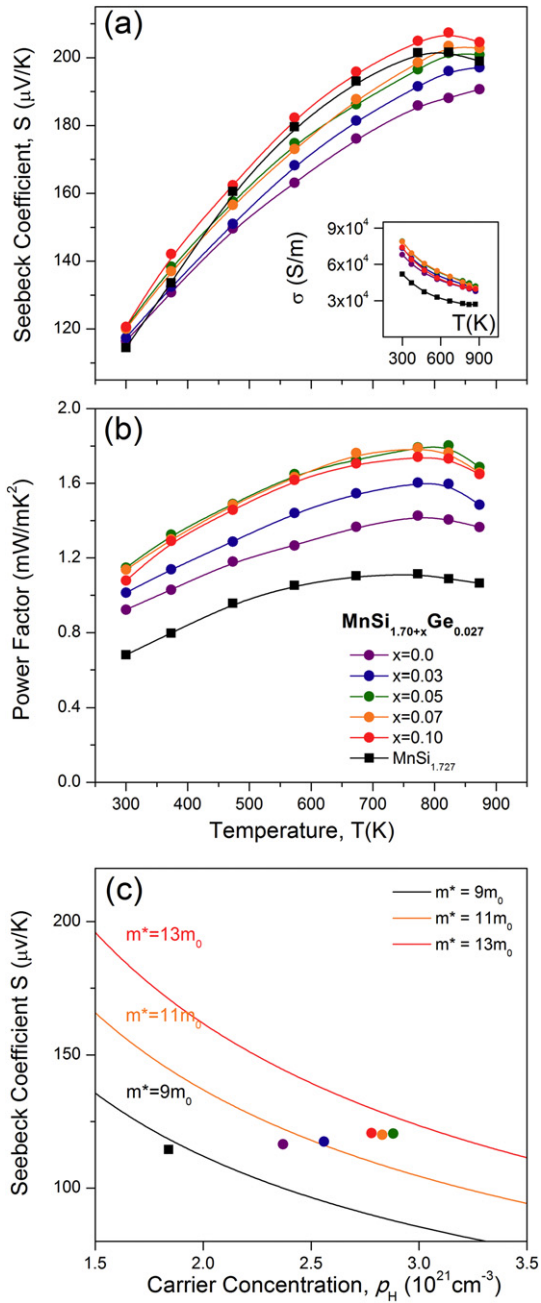| Samples	Secondary phases			Density
	MnSi (wt%)	Si (wt%)	Total (wt%)	(g/cm^3)
x = 0.0	5.13	0.35	5.48	5.06
x = 0.03	4.16	0.78	4.94	4.98
x = 0.05	1.67	0.85	2.52	4.91
x = 0.07	1.13	0.81	1.93	4.87
x = 0.10	0.25	1.22	1.47	4.82

Fig. 2. Temperature dependences of (a) Seebeck coefficient and (b) power factor for Ge-HMSs and pristine MnSi$_{1.727}$. The inset in (a) shows the temperature dependence of electrical conductivity. (c) Seebeck coefficient as a function of carrier concentration (Pisarenko plot) at 300 K for Ge-HMSs and pristine MnSi$_{1.727}$.

within the temperature range used for measurement, owing to increased p_H caused by Ge-doping. The enhanced power factor values of Ge-HMSs when compared to the pristine sample (Fig. 2(b)), can be

Table 2
Hall coefficient R_H, Hall carrier concentration p_H, Hall mobility μ_H and effective mass m_d^* at 300 K for pristine MnSi$_{1.727}$ and MnSi$_{1.70 + x}$Ge$_{0.027}$.

Samples	R_H (10^{-9} m^3 C^{-1})	p_H (10^{21} cm^{-3})	μ_H (cm^2 V^{-1} s^{-1})	m_d^*/m_0
MnSi$_{1.727}$	3.34	1.84	1.74	8.7
x = 0.0	2.60	2.37	1.77	10.5
x = 0.03	2.40	2.56	1.77	11.1
x = 0.05	2.14	2.88	1.76	12.3
x = 0.07	2.17	2.83	1.71	12.2
x = 0.10	2.21	2.78	1.64	12.1

attributed to the increase in density of states effective mass m_d^*, as reported in previous studies [10–12]. On the other hand, the electronic transport properties depend on the Si content, as shown in Fig. 2. From x = 0 to x = 0.05 in MnSi$_{1.70 + x}$Ge$_{0.027}$, the σ values increase with Si content mainly because of the increase in p_H (inset of Fig. 2(a)). The variation of p_H values, ranging from 2.37×10^{21} cm^{-3} (x = 0) to 2.88×10^{21} cm^{-3} (x = 0.05), with Si content is likely to be related with the presence of secondary phases (MnSi and Si) and Si vacancies. For samples with x = 0.07 and x = 0.1, the σ values slightly decreased when compared to the sample with x = 0.05 owing to the decrease in both p_H and μ_H (Table 2). A further study on the carrier concentration with defect structures and their effects on the electronic and thermal transport properties of HMSs will be necessary in near future.

On the other hand, all HMSs including pristine MnSi$_{1.727}$ exhibit positive S values, indicating p-type semiconductors. As expected, the S values of the sample with x = 0 are smaller than those of the pristine sample mainly because of the increase in p_H, while S values of the Ge-HMSs are improved with increasing Si content, despite of the increase in p_H (Fig. 2(a)). This difference in electronic transport characteristics can also be seen in the power factor data. Fig. 2(b) shows the temperature dependence of the calculated power factor values for the pristine and Ge-HMS samples. Power factor values are enhanced by Ge-doping and Si-content tuning; the power factor value saturated at x = 0.05, showing a maximum value of 1.8 mW m^{-1} K^{-2} at 823 K, which is 66% higher than that of pristine MnSi$_{1.727}$. This result indicates that the electronic structure of the HMSs can be changed by controlling the Si content as well as the Ge-doping. To elucidate this, we calculated the m_d^* values at 300 K as represented in Fig. 2(c) and Table 2. The m_d^* was estimated using Eq. (1) as follows [18].

$$S = \frac{8\pi^2 k_B^2}{3eh^2}\left(\frac{\pi}{3p_H}\right)^{2/3} m_d^* T \qquad (1)$$

Here, k_B, e, and h are the Boltzmann constant, elementary charge, and the Planck's constant, respectively. Fig. 2(c) shows the measured S as a function of p_H (Pisarenko plot) at 300 K. The solid lines are calculated for $m_d^* = 9.0$, 11.0, and $13.0m_0$ using the SPB model and energy-independent carrier scattering approximation for degenerated semiconductors. As shown in Fig. 2(c) and Table 2, m_d^* increases from $8.7m_0$ (pristine MnSi$_{1.727}$) to $10.5–12.3m_0$ (Ge-HMSs) because of Ge-doping and Si-content tuning.

The temperature dependence of κ and κ_{lat} for pristine MnSi$_{1.727}$ and the Ge-HMSs is shown in Fig. 3(a). The κ value for Ge-HMSs is slightly higher than that for MnSi$_{1.727}$ mainly because of the increase in electronic contribution (κ_{ele}). To verify the phonon scattering effect because of point defects (Ge$_{Si}$) and secondary phases (MnSi and Si), we calculated the κ_{lat} values by subtracting κ_{ele} from κ. The κ_{ele} values were estimated using the Wiedemann–Franz law ($\kappa_{ele} = L\sigma T$). The Lorenz number (L) is obtained from Eq. (2) and is approximately 1.8×10^{-8} V^2 K^{-2}.

$$L = \left(\frac{k_B}{e}\right)^2 \left(\frac{(r + 7/2)F_{r+5/2}(\eta)}{(r + 3/2)F_{r+1/2}(\eta)} - \left[\frac{(r + 5/2)F_{r+3/2}(\eta)}{(r + 3/2)F_{r+1/2}(\eta)}\right]^2\right) \qquad (2)$$

where r is the scattering parameter from the temperature dependence of μ_H and $F_n(\eta)$ is the Fermi integral of a Fermi level function η. The calculated value of κ_{lat} also includes bipolar thermal conduction; thus, we compared the κ_{lat} values of the Ge-HMSs at 300 K to minimize the bipolar effect. As shown in Fig. 3(a), κ_{lat} values were slightly decreased both by Ge doping (point defect phonon scattering due to the mass difference between Si (M$_{Si}$ ~ 28.08) and Ge (M$_{Ge}$ ~ 72.63)) and the reduced secondary phases with higher κ (κ_{MnSi} ~ 11.5 W m^{-1} K^{-1} and κ_{Si} ~ 145 W m^{-1} K^{-1} at 300 K) [19,20]. The temperature dependences of ZT for pristine MnSi$_{1.727}$ and the Ge-HMSs are shown in Fig. 3(b). The highest ZT value obtained is 0.61 at 823 K for MnSi$_{1.77}$Ge$_{0.027}$, which indicates a 33% enhancement when compared to MnSi$_{1.70}$Ge$_{0.027}$. Although κ_{lat} values were not significantly decreased by Si-content
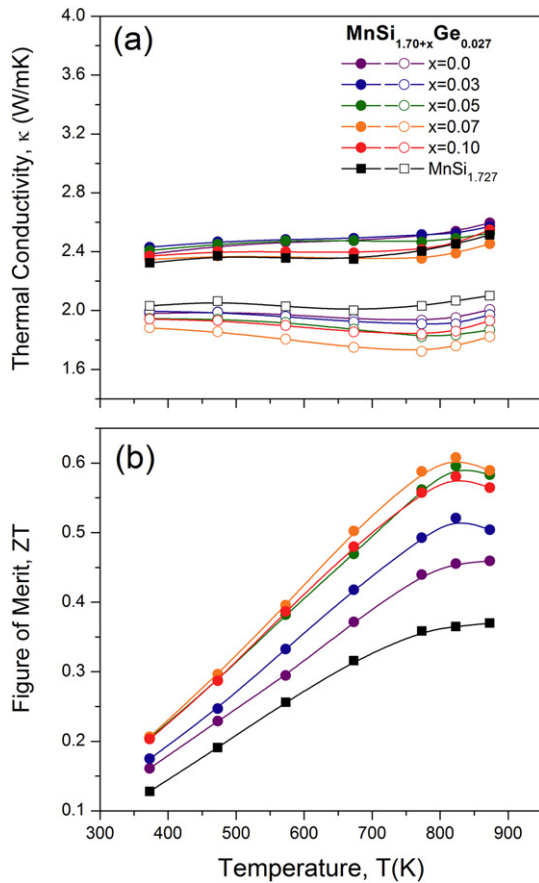
Fig. 3. Temperature dependences of (a) the total thermal conductivity κ (solid) and the lattice thermal conductivity κ_{lat} (open) and (b) figure of merit ZT for Ge-HMSs and pristine $MnSi_{1.727}$.

tuning, ZT increased owing to the enhancement of the power factor, which resulted from the electronic structure modification because of the varying Si content.

4. Conclusions

We found Si-content tuning to be a critical processing parameter for the fabrication of thermoelectric HMSs with a high ZT by controlling phase formation behavior. The generation of secondary phases (MnSi and Si) and Si vacancy is effectively controlled by optimizing Si content, and this resulted in simultaneous enhancement of carrier transport and

phonon scattering. The evaluation of electronic and thermal transport parameters suggests that the electronic structure could be modified by adjusting Si-site occupancy, leading to a significant enhancement of the power factor because of the increased density of states effective mass. As a consequence, a maximum ZT of 0.61 is obtained at 823 K for $MnSi_{1.77}Ge_{0.027}$. This simple and effective compositional tuning approach for controlling the phase formation behavior, closely related with the thermoelectric transport properties, provides an insight into the synthesis of Si-based thermoelectric materials.

References

[1] B.C. Sales, D. Mandrus, R.K. Williams, Science 272 (1996) 1325–1328.
[2] Y. Tang, R. Hanus, S. Chen, G.J. Snyder, Nat. Commun. 6 (2015) 7584.
[3] J. Yang, H. Li, T. Wu, W. Zhang, L. Chen, J. Yang, Adv. Funct. Mater. 18 (2008) 2880–2888.
[4] G. Kim, J. Kim, H. Lee, S. Cho, I. Lyo, S. Noh, B.W. Kim, S.W. Kim, K.H. Lee, W. Lee, Scr. Mater. 116 (2016) 11–15.
[5] X. Liu, T. Zhu, H. Wang, L. Hu, H. Xie, G. Jiang, G.J. Snyder, X. Zhao, Adv. Energy Mater. 3 (2013) 1238–1244.
[6] I. Nishida, Phys. Rev. B 7 (1973) 2710–2713.
[7] D. Shinoda, S. Asanabe, Y. Sasaki, J. Phys. Soc. Jpn. 19 (1964) 269–272.
[8] I. Nishida, J. Mater. Sci. 7 (1972) 435–440.
[9] Y. Miyazaki, D. Igarashi, K. Hayashi, T. Kajitani, K. Yubuta, Phys. Rev. B 78 (2008) 214104.
[10] A.J. Zhou, T. Zhu, X.B. Zhao, S.H. Yang, T. Dasgupta, C. Stiewe, R. Hassdorf, E. Mueller, J. Electron. Mater. 39 (2010) 2002–2007.
[11] X. She, X. Su, H. Du, T. Liang, G. Zheng, Y. Yan, R. Akram, C. Uher, X. Tang, J. Mater. Chem. C 3 (2015) 12116–12122.
[12] H. Lee, G. Kim, B. Lee, K.H. Lee, W. Lee, J. Electron. Mater. (2016) http://dx.doi.org/10.1007/s11664-016-5035-y.
[13] X. Chen, J. Zhou, J.B. Goodenough, L. Shi, J. Mater. Chem. C 3 (2015) 10500–10508.
[14] X. Chen, S.N. Girard, F. Meng, E. Lara-Curzio, S. Jin, J.B. Goodenough, J. Zhou, L. Shi, Adv. Energy Mater. 4 (2014) 1400452.
[15] V. Ponnambalam, D.T. Morelli, S. Bhattacharya, T.M. Tritt, J. Alloys Compd. 580 (2013) 598–603.
[16] G. Bernard-Granger, M. Soulier, H. Ihou-Mouko, C. Navone, M. Boidot, J. Leforestier, J. Simon, J. Alloys Compd. 618 (2015) 403–412.
[17] D.Y. Nhi Trung, D. Berthebaud, F. Gascoin, H. Kleinke, J. Electron. Mater. 44 (2015) 3603–3611.
[18] G.J. Snyder, E.S. Toberer, Nat. Mater. 7 (2008) 105–114.
[19] J.G. Cheng, F. Zhou, J.S. Zhou, J.B. Goodenough, Y. Sui, Phys. Rev. B 82 (2010) 214402.
[20] P.D. Maycock, Solid State Electron. 10 (1967) 161–168.